

# Incipient instability in free convection laminar boundary layers

By **CONSTANTINE E. POLYMEROPOULOS**

Rutgers University

AND **BENJAMIN GEBHART**

Cornell University

(Received 16 February 1967 and in revised form 23 May 1967)

This paper presents the results of an experimental investigation of the behaviour of artificial disturbances produced by an oscillating ribbon in the free convection boundary layer over a vertical uniform flux plate. The boundary layer was observed using a Mach Zehnder interferometer. The observations resulted in the approximate location of a neutral curve which is in good agreement with calculations from the linear stability theory.

---

## I. Introduction

The stability of laminar flows has attracted investigators for many years because of its importance in the mechanism of transition to turbulence. For the case of free convection over a vertical uniform flux plate Polymeropoulos & Gebhart (1966) computed part of the neutral curve from the linear stability theory and compared the results with similar computations for a uniform temperature plate.

Experimental investigations on the stability of the free convection boundary layer over a vertical flat plate have involved observations of both natural and artificial oscillations. Experiments on the transition to turbulence using a uniform temperature plate in air were performed by Herman (1936) and Saunders (1939) using the schlieren and the shadowgraph method respectively. Eckert & Soehngen (1951) investigated the onset of natural oscillations and the transition to turbulence in air using a Mach Zehnder interferometer. Mordchelles-Regnier & Kaplan (1963) observed the onset of instabilities in carbon dioxide under pressure using a differential interferometer, and Szewczyk (1962) investigated naturally occurring oscillations in water using a dye injection method. The onset of instabilities for the case of a uniform flux plate in pressurized nitrogen was observed interferometrically by Polymeropoulos (1966). The results of these studies showed considerable difference in the Grashof number for the onset of instabilities as compared with that predicted by the theory, presumably because the natural oscillations are too small to be detected at their initial stages of amplification. Consequently, the observation of natural oscillations alone did not furnish any definite information either on the location of the neutral curve, or on the question of the applicability of conventional stability theory to free convection boundary layer flows.

A method for testing the predictions of the stability theory that has been used successfully for the forced flow over a flat plate by Schubauer & Skramstad (1948) and others, is that of producing artificial oscillations inside the boundary layer. These can be large enough to be easily detected, and their wave-number can be varied to check the entire neutral curve diagram. Birch (1957) and Gartrell (1959) attempted to use such oscillations for the free convection flow over a uniform temperature plate, but their results were inconclusive. Hollman, Gartrell & Soehngen (1959) performed measurements on amplified artificial oscillations without attempting to locate a neutral stability curve. Colak-Antic (1964) measured amplitude distributions of artificial oscillations, and found qualitative evidence for the existence of a buoyancy coupling effect at low Grashof and wave-numbers. The effect of obstructions in the boundary layer was studied by Hollman, Stout & Soehngen (1960) and by Eckert, Hartnett & Irvine (1960). In the latter paper it was also reported that visual observations of smoke threads showed that natural oscillations were two-dimensional when they were first observed.

The purpose of this paper is to present experimental evidence for the location of the neutral curve for free convection flow over a uniform flux plate. Artificial oscillations were produced by means of an oscillating ribbon and the flow was observed using a Mach Zehnder interferometer.

Observations were performed in the range of  $G < 675$ , which is lower than the condition of first observation of natural oscillations (approximately  $G = 675$  (Polymeropoulos 1966)), but spans the most important part of the predicted neutral curve, which is at relatively low values of  $G$ .  $G$  is a Grashof number parameter given by  $G = 5[\text{Gr}'_x/5]^{\frac{1}{2}}$ , where  $\text{Gr}'_x = g\beta q''x^4/k\nu^2$  is the modified Grashof number for the uniform flux plate (appendix A),  $q''$  is the heat flux,  $x$  is the distance along the plate,  $\beta$  is the coefficient of volume expansion,  $g$  the gravitational constant, and  $k$  and  $\nu$  the thermal conductivity and the kinematic viscosity respectively.

## 2. Experimental apparatus

The test surface was a flat plate consisting of two pieces of 2 in. by 12 in. by 0.0005 in. Inconel 600 foil glued together by a thin coat of contact cement. They were clamped at the ends and stretched vertically between two brass clamps. The brass clamps were fastened on a Lucite piece, so that one end of the foil gave a 45° leading edge effect, while the other was at an angle of 90° to the brass clamps. The foil was electrically heated through electrodes attached to the brass clamps. It was placed in a tank certified for pressures to 18 atmospheres, and the free convection boundary layer was observed through 1 in. by 8 in. vertical slit windows using the 20 cm Mach Zehnder interferometer described by Gebhart & Knowles (1966). A compensating tank was used for equalizing the path lengths. The windows were glass plates 9 in. long, 2 in. wide and 2 in. thick held against O rings by means of the inside pressure of the tanks. Prepurified oil-free nitrogen was used for pressurization.

The interferometer output was observed through an optical system which

changed the aspect ratio from 8:1 to 5:4. A similar optical system for a schlieren system was described by Buchele & Goosens (1954). The foil was aligned in the interferometer field by means of a mechanism internal to the test tank. Data were collected using still and motion picture photography. A digital timer was used to record the time lapse on the motion pictures. To check the uniform flux boundary condition on the foil, as well as its surface temperature, the measured temperature distribution along the foil, obtained by counting the fringes from interferograms and using a classical value of the Dale-Gladstone constant, was compared with the results of the boundary-layer solution of Sparrow & Gregg (1956). The boundary layer equations are shown in appendix A. Within the range of pressures (approximately 43–255 psia) and average foil temperature excesses (approximately 10–70 °F) that were used during the stability observations, the maximum difference between the experimental and calculated surface temperature distribution for the same condition was 8%. The average difference was 4%. Since relatively large errors in the foil conditions can be tolerated in the computation of the Grashof number parameter  $G$ , this agreement was considered satisfactory.

The introduction of controlled disturbances into the boundary layer was accomplished by means of a small ribbon which was made to oscillate perpendicular to the foil at adjustable frequencies and amplitudes inside the boundary layer. The ribbon was made of a piece of Nichrome V foil, 4 in. wide,  $\frac{1}{16}$  in. high, and 0.001 in. thick, soldered on a V brass support. The orientation of the ribbon was parallel to the foil surface and the foil leading edge.

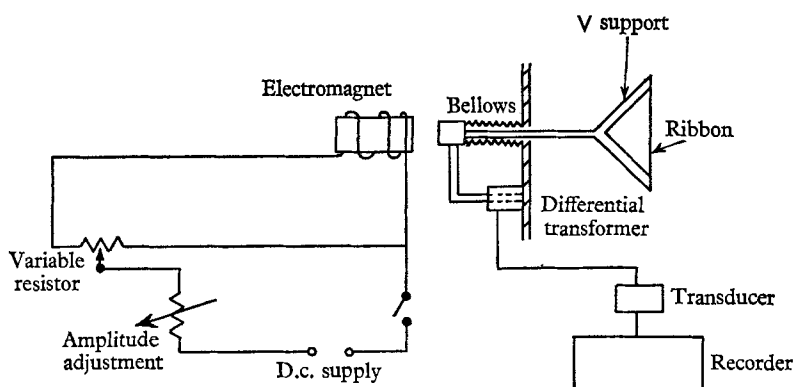


FIGURE 1. Schematic diagram of the disturbance generator.

Figure 1 shows a schematic diagram of the disturbance generator. The ribbon was given a sinusoidal type motion, by applying a nearly sinusoidal voltage to an electromagnet which exerted a force on a bellows spring-loaded iron plunger, attached to the V brass support of the ribbon. The voltage variation was provided by the motion of a variable resistor, connected through a three-linkage mechanism and reduction gear box to a variable speed motor. The amplitude of the voltage oscillation could be adjusted either by changing the voltage output of the d.c. power supply, or by means of a variable resistor in series with the power supply. The motion of the ribbon was recorded using a differential trans-

former whose output was recorded using an Offner recorder. Figure 2 shows a record of the ribbon motion for an amplitude of 0.002 in. and 8 c/s. The motion of the ribbon was only approximately sinusoidal because of the use of the three-linkage mechanism, and the friction and inertia of the system.

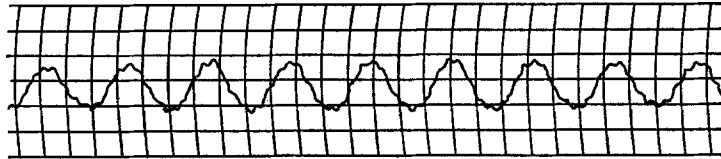


FIGURE 2. Record of the ribbon motion. Frequency: 8 c/s. Amplitude: 0.002 in. approximately.

### 3. Experimental procedure and results

#### *Effect of the ribbon in the boundary layer*

The presence of the ribbon in the boundary layer resulted in a localized disturbance of the base free convection flow. Figure 3 is a typical comparison of the position of the isotherm passing through the tip of the ribbon with the corresponding isotherm on the opposite side of the foil. It shows that at a relatively short distance downstream from the ribbon the flow returned to its undisturbed temperature condition.

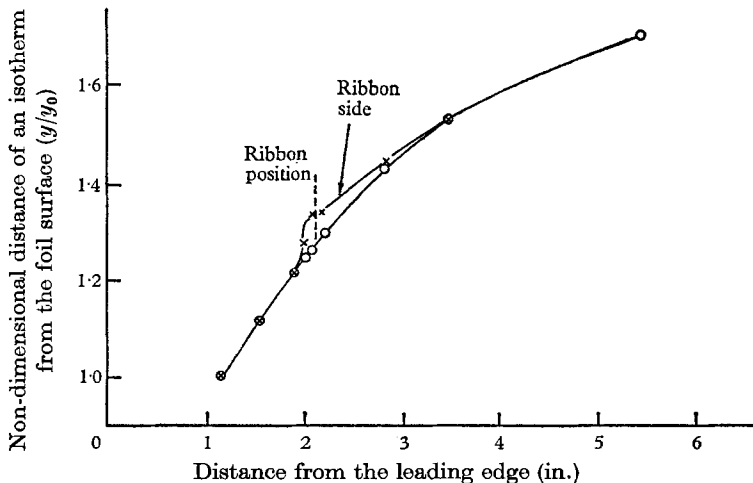


FIGURE 3. Isotherm passing through the tip of the ribbon compared with the corresponding isotherm on the other side of the foil. At  $x = 1.2$  in. the distance of this isotherm from the foil was set equal to 1.0. The ribbon is at the inflexion point ( $\eta = 1.65$ ).  $G = 166$  at the ribbon.

Oscillations of the ribbon produced waves travelling with respect to the fringe pattern that defined the base flow boundary layer. Such waves amplified or damped depending on the ribbon frequency and upon the local stability or

instability of the boundary layer. Amplification is defined as the spatial increase in wave amplitude as measured from interferograms. Examples of amplified and damped waves are shown on figures 6*a* and 6*b*, plate 1. The quantity  $\alpha$  given in connexion with the figures is the non-dimensional wave-number of the oscillations,  $\alpha = 10\pi x/\lambda G$ , where  $\lambda$  is the wavelength. Table 1 contains the data pertaining to the interferograms.

---

Figure	Pressure (psia)	Temperature (°F)	Frequency (c/s)	Heat flux (B.Th.U./ h ft. <sup>2</sup> )	Distance of ribbon from leading edge (in.)
6 <i>a</i>	227.7	76	3.0	45.6	2.88
6 <i>b</i>	227.7	76	11.5	45.6	2.88
6 <i>c</i>	51.5	76	4.4	86.8	1.55
6 <i>d</i>	136.7	75	6.2	41.5	4.90
6 <i>e</i>	160.7	74	6.1	55.5	5.35
6 <i>f</i>	78.2	75	9.0	84.8	4.89
6 <i>g</i>	76.1	74	4.1	70.6	2.01

TABLE 1. Data for the interferograms shown on figure 6

---

The effect of the distance of the oscillating ribbon from the foil surface was checked by traversing it normal to the foil at fixed distances from the leading edge and for fixed flow conditions, i.e.  $G$ . The amplitude of the ribbon oscillation was kept constant and at a very small value (approximately 0.5% of the boundary-layer thickness). At each position the ribbon frequency was increased from approximately 0.8 c/s to the highest frequency,  $c$ , for which oscillations were visible along the entire length of the foil, downstream from the ribbon. The distance of the ribbon from the foil surface was measured by counting the number of fringes from the foil to the ribbon, and then using the computed base flow temperature distribution to convert to the corresponding value of the similarity variable  $\eta$  (appendix A). Figure 4 shows the results of one such traverse. The maximum frequency for amplification for this traverse was at  $\eta = 1.75$ , which is close to the inflexion point of the theoretical velocity profile ( $\eta = 1.65$ ). Repeated traverses in the range of conditions used for stability observations showed the maximum frequency favoured at locations within  $\pm 10\%$  of the inflexion point. Computations for the uncoupled neutral curve, performed by the authors (1966) in the range of  $180 > G > 125$  showed that, in the vicinity of the neutral curve, the outer critical layer location ranges over  $\eta$  values near those of the base flow inflexion point location. This behaviour also confirms the observations of Szewczyk (1962) on the importance of the outer critical layer on stability. There was no attempt to find a minimum frequency for amplification because of the long wavelengths involved with low disturbance frequencies.

In view of these experimental results, the ribbon was placed at the position corresponding to the inflexion point of the local base flow velocity profile for all subsequent stability determinations. This resulted in experimental data on the

upper branch of the theoretical neutral curve, since for a given set of conditions, i.e.  $G$ , the maximum frequency for amplification results in the maximum wave-number for amplification.

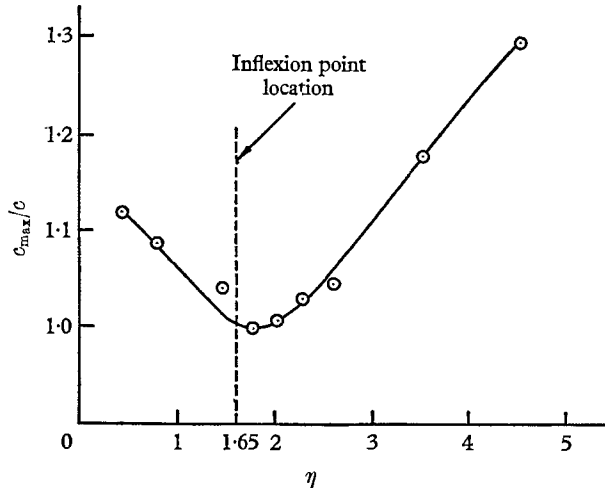


FIGURE 4. Effect of the ribbon distance from the foil.  $c_{\max}$  is the maximum frequency for amplification for this traverse across the boundary layer.  $c$  is the maximum frequency for amplification for each local ribbon position in the boundary layer.  $G = 131$  at the ribbon.

#### *Measurement of oscillation parameters*

Measurements were obtained from motion pictures projected on a ground glass screen, or from still pictures using an optical comparator. Scaling in the vertical direction was from thin horizontal wires in the field whose distance from each other and from the leading edge was known. Wave amplitudes were determined by subtracting the maximum from the minimum distance from the foil for each wave defined by the interference fringes. These were used only for qualitative comparisons of amplitude change along the foil.

Large ribbon amplitudes (0.04 in.) produced waves at the ribbon whose initial amplitude was as high as 20% of the boundary layer thickness. Such large wave amplitudes may not agree with the infinitesimal disturbances used in the hydrodynamic stability theory, but were necessary for accurate comparisons of downstream wave amplitude change. The downstream wavelength and frequency of the oscillations were not affected by their amplitude. No significant change in frequency or wavelength could be detected across the boundary layer. This is perhaps because the wave amplitude was too small to be observed with high accuracy very near the foil ( $\eta < 0.4$ ) and at the outermost parts of the boundary layer ( $\eta > 2.8$ ) where owing to the small velocity of the base flow the ribbon motion would produce distinctly smaller wavelengths.

Figure 5 shows the measured change of  $\alpha$  with  $x$  along the foil for several different tests. The value of  $\alpha$  at the ribbon was obtained by extrapolation from the values measured on interferograms downstream from the ribbon. The dotted lines on figure 5 indicate the extrapolation process. One may calculate the  $\alpha, x$

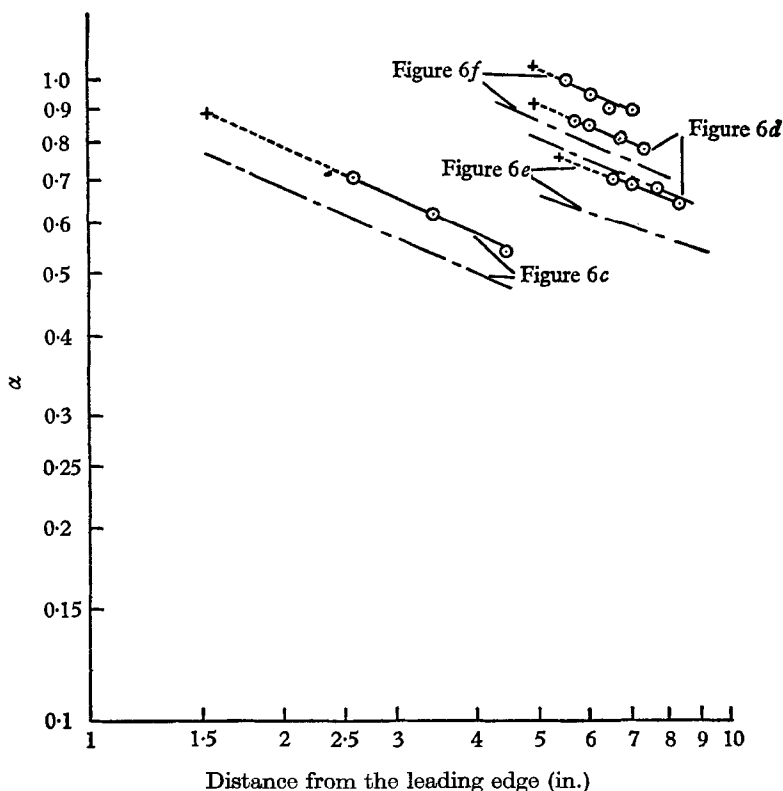


FIGURE 5. Variation of  $\alpha$  along the foil. Dotted lines indicate extrapolation. — — —, equation (1); +, ribbon position.

relationship using the definition of  $\alpha$ , the relationship  $\lambda = u/c$  for the wavelength, and the definitions of  $f'$ ,  $G$  and,  $Gr'_x$  in appendix A:

$$\alpha = \frac{2\pi c x^{-\frac{2}{5}}}{5\nu f' \left( \frac{g\beta q''}{5k\nu^2} \right)^{\frac{2}{5}}} \tag{1}$$

$u$  is the velocity of the oscillations. The two-fifths slope indicated by (1) agrees with the slope of the experimental points. As seen on figure 5 there is a difference between (1), computed using for  $f'$  the non-dimensional base flow velocity at the inflexion point, and the experimental values of  $\alpha$ . This is because in general the waves travel with a velocity different than that of the inflexion point. The paths on the  $(\alpha, G)$ -plane for the tests shown on figure 5 are drawn on figure 8.

*Neutral stability measurements*

The most convincing experimental proof for the existence of a neutral curve is furnished by oscillations which are initially damped and subsequently amplified as they travel downstream or vice versa. The regions where the oscillations change from damped to amplified, or vice versa, give estimates of the position of the neutral curve.

Interferograms of oscillations which are initially damped and then amplified could be obtained showing transition from damping to amplification in the range of  $182 < G < 315$ . Figure 6c, plate 1, is an interferogram of such a case. Figure 7 shows the measured amplitude distribution across the boundary layer for successive downstream positions, measured from the photograph on figure 6c. These amplitude distributions clearly show the change from damping to amplification. The conditions tested are shown on figure 8 as the squares. The estimated accuracy of the data points in  $\alpha$  and  $G$  is indicated by the limiting lines around the points. The data are listed on table 2.

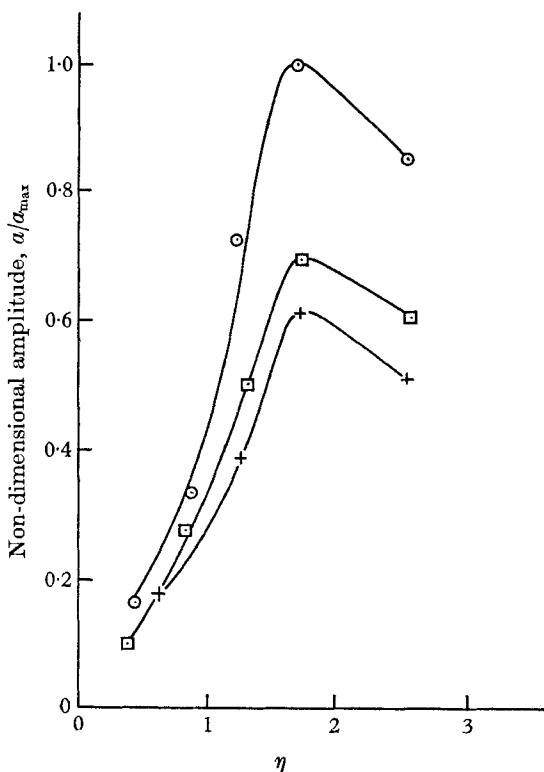


FIGURE 7. Amplitude measurements from oscillations on figure 6c. Distances from the leading edge: ○, 2.6 in.; +, 3.3 in.; □, 4.4 in.  $a_{max}$  is the maximum measured amplitude for these traverses.

It was not possible to obtain any experimental points showing both damping and then amplification in the range of  $G < 182$  because the wavelengths were too long. Approximately two damped waves after the ribbon are necessary in order to observe the transition from damping to amplification. This would require placing the ribbon at very small values of  $G$ . For oscillations at small values of  $\alpha$  and  $G$  the resulting wavelengths are large compared with the distance from the leading edge. The flow curvature at low values of  $G$  and the long wavelengths made accurate observations of wave amplitude change very difficult.

Pressure (psia)	Temperature (°F)	Heat flux (B.Th.U./ h ft. <sup>2</sup> )	Frequency (c/s)	Distance of ribbon from leading edge (in.)	Change from damped to amplified, or vice versa (in.)	$\lambda$ at the position of change (in.)	$\alpha$ at the position of change	$G$ at the position of change
51.5	76	86.8	4.4	1.55	3.44	0.79	0.62	217
73.2	73	93.4	7.0	2.10	4.35	0.56	0.78	315
75.5	75	93.3	5.9	1.64	3.80	0.56	0.75	283
49.7	75	111.0	6.1	2.04	4.25	0.69	0.74	263
51.7	72	83.2	5.2	1.22	2.72	0.80	0.59	182
41.2	75	47.9	3.6	1.52	4.44	1.03	0.63	215
122.0	75	50.0	5.8	4.94	7.00	0.56	0.79	500
75.7	76	53.6	5.7	5.38	7.31	0.57	0.78	515
136.7	75	41.2	6.2	4.90	6.59	0.53	0.82	467
136.7	75	39.4	5.2	4.90	6.59	0.57	0.81	442

TABLE 2. Data for tests where change from damping to amplification, or vice versa, was observed

Oscillations showing a transition from amplification to damping were observed during several tests in the range of  $442 < G < 515$ . This behaviour was thought to result from crossing the neutral stability curve from the unstable to the stable region. The experimental points are shown as triangles on figure 8, and are presumably near the neutral stability curve. Table 2 lists the data, and figure 6*d*, plate 1, shows an interferogram of such oscillations. Figure 9 shows the change from amplification to damping from amplitude distributions measured at successive downstream positions across the boundary layer. Figures 6*e* and 6*f*, plate 2, show amplified and damped oscillations in approximately the same range of  $G$  as the oscillations on figure 6*d*, plate 1. The paths of the oscillations on the  $(\alpha, G)$ -plane are also indicated on figure 8. These clearly show the existence of stable and unstable regions above and below the position of the experimental points (triangles) of transition from amplification to damping. They also indicate that in the range of  $442 < G < 515$  the neutral curve has a negative slope which is steeper than the slope of the line defining the oscillation paths on the  $(\alpha, G)$ -plane.

An approximate location of the neutral curve can be drawn using the experimentally observed behaviour referred to above. This is shown on figure 8. In the range of  $315 < G < 442$ , where no experimental points are available, the curve was drawn to fit the data in the adjacent ranges of  $G$ . This is shown as the dotted portion of the curve on figure 8.

The previously computed neutral stability curves are compared on figure 10 with the experimental results. Appendix B shows the equations for the conversion of the computed neutral stability curves for a uniform temperature plate to those for a uniform flux plate. The former are reasonable approximations for the latter (Polymeropoulos & Gebhart 1966). The agreement of the experimental data with the theory is good, although the experimental points are located inside the region predicted to be unstable by the theory.

#### *Neutral stability measurements by approximate methods*

Observations of the change from damping to amplification, or vice versa, did not provide stability information at low values of  $\alpha$  and  $G$ . Different methods were

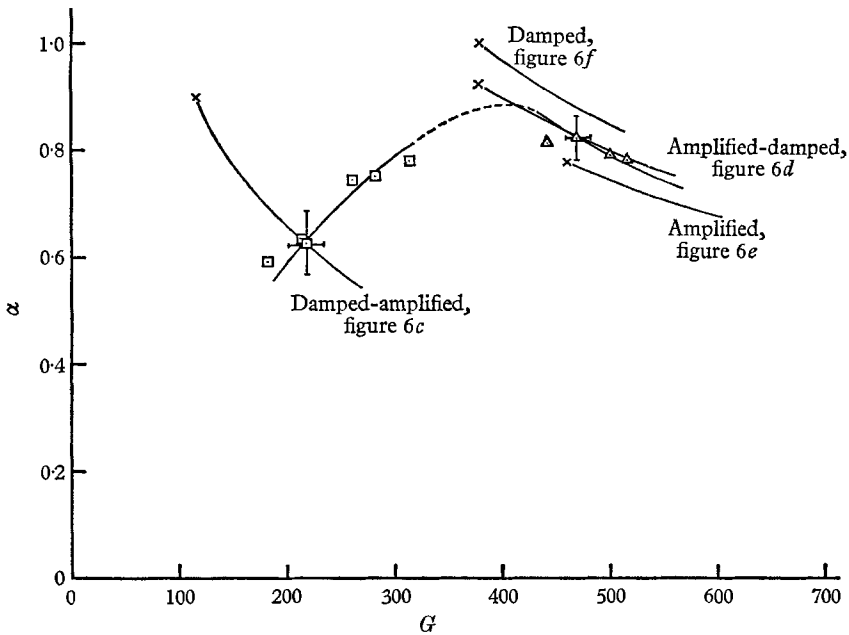


FIGURE 8. Experimental points showing transition from amplification to damping, or vice versa:  $\square$ , damped-amplified;  $\triangle$ , amplified-damped;  $\times$ , ribbon position.

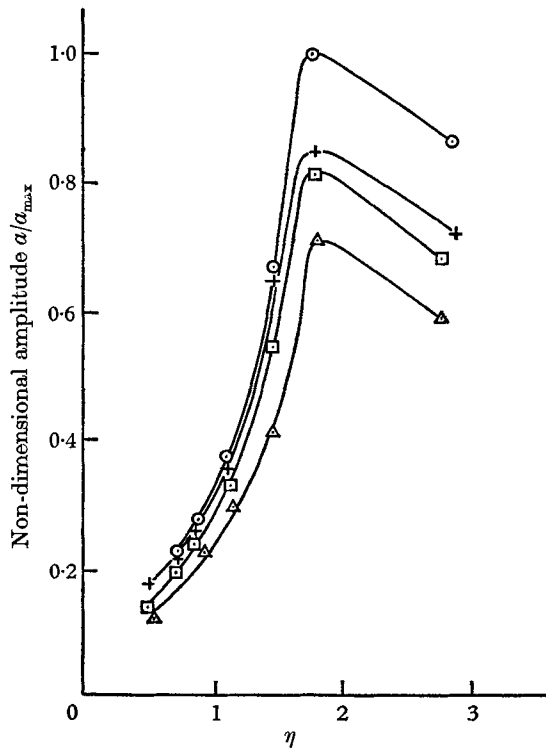


FIGURE 9. Amplitude measurements from oscillations on figure 6d. Distances from the leading edge:  $\square$ , 5.5 in.; +, 5.9 in.;  $\odot$ , 6.4 in.;  $\triangle$ , 7.0 in.  $a_{max}$  is the maximum measured amplitude for these traverses.

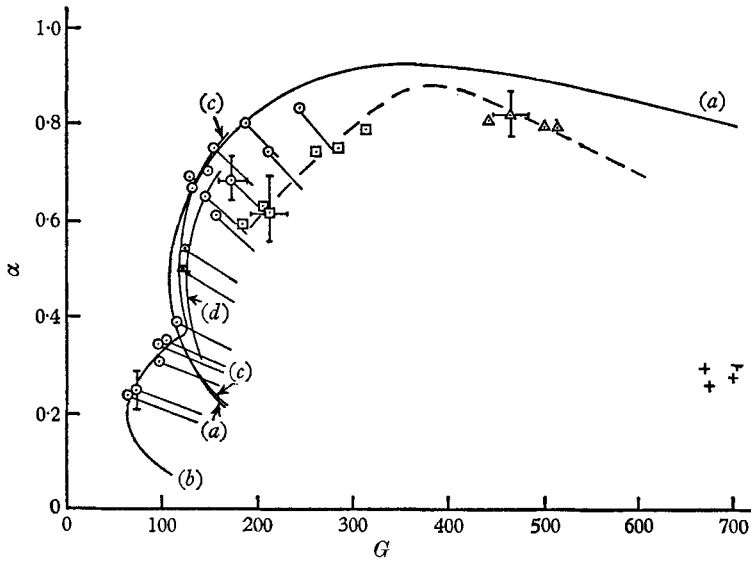


FIGURE 10. Comparison of the experimental results with the previous results of stability computations. (a) Kurtz & Crandall (1961), uncoupled, (b) Nachtsheim (1963), coupled, (c) Nachtsheim (1963), uncoupled, and (d) Polymeropoulos & Gebhart (1966), uncoupled. +, natural oscillations, Polymeropoulos (1966);  $\square$ , damped-amplified;  $\triangle$ , amplified-damped;  $\odot$ ,  $\ominus$ , approximate methods.

therefore adopted which were qualitative but which gave important evidence concerning the conditions for flow instability.

The ribbon position  $\alpha$ , tank pressure and foil heating rate were adjusted so that the value of  $G$  at the ribbon was near the suspected neutral curve. Using a small ribbon amplitude (approximately 0.001 in., or 0.5% of the boundary-layer thickness) the frequency was changed until a mean frequency level was reached from which changes of approximately  $\pm 5\%$  could make the waves produced by the ribbon continue, or disappear along the entire visible length of the foil. The changes in frequency resulted in displacements of the ribbon position parallel to the  $\alpha$ -axis on the  $(\alpha, G)$ -plane. They were thought to result in amplified and damped oscillations originating in the vicinity of the stable and unstable regions of the  $(\alpha, G)$ -plane respectively. At the mean frequency level the oscillations produced by the ribbon were thought to originate near the neutral curve. Figure 6*g*, plate 2, is an interferogram of such oscillations. The photograph was taken with a ribbon amplitude increased to approximately 20% of the boundary layer thickness. The experimental points obtained by this method are shown as circles on figure 10.

The region of sudden increase in  $\alpha$ , predicted by the theory in the vicinity of  $G = 125$ , could not be checked by the above technique. It was therefore necessary to move in  $\alpha$  and  $G$ , at a given ribbon frequency, by changing the foil current. Two experimental points that were obtained in this manner are shown as the half circles on figure 10 and are in good agreement with the rest of the results. Table 3 lists the data and measured parameters for the experimental points obtained using the approximate methods.

Pressure (psia)	Tempera- ture (°F)	Heat flux (B.Th.U./ h ft. <sup>2</sup> )	Frequency (c/s)	Distance of ribbon from leading edge (in.)	$\lambda$ at the ribbon (in.)	$\alpha$ at the ribbon	$G$ at the ribbon
43.2	76	72.4	1.5	0.88	1.65	0.24	68
50.1	76	72.4	1.6	0.88	1.52	0.25	72
49.7	75	109.0	2.5	1.17	1.12	0.34	97
41.2	74	111.0	2.6	1.30	1.31	0.32	98
43.7	75	42.2	2.0	1.75	1.49	0.35	105
48.7	75	55.5	2.2	1.75	1.25	0.38	115
55.7	75	56.7	2.5	1.75	0.92	0.49	121
56.7	74	60.8	3.1	1.75	0.81	0.54	125
56.7	76	72.1	3.8	1.75	0.62	0.69	129
54.2	75	83.9	4.0	1.75	0.63	0.67	131
75.5	75	62.3	3.6	1.69	0.60	0.65	141
74.2	77	70.2	4.0	1.75	0.54	0.71	143
84.7	76	88.8	4.9	1.75	0.46	0.76	158
76.1	75	70.6	4.1	2.01	0.65	0.61	160
89.7	76	48.7	3.6	2.20	0.60	0.67	172
89.7	75	80.7	4.7	2.20	0.46	0.80	189
87.7	75	72.7	5.4	2.63	0.52	0.74	216
122.7	74	72.7	6.1	2.63	0.41	0.83	245

TABLE 3. Data for tests using approximate methods

An oscillation originating in the stable region of the  $(\alpha, G)$ -plane could appear to be amplified, if it reached the unstable region before the damping became evident, i.e. before travelling a distance of approximately two wavelengths. It would therefore be expected that the experimental unstable points obtained from the approximate methods probably lie in the stable portion of the  $(\alpha, G)$ -plane. To minimize this effect the ribbon amplitudes were very small (0.001 in.) so that with a small amount of damping the waves would not be visible within a short distance from the ribbon. To obtain an estimate of this uncertainty we assumed that the experimental points were in the stable region. The change in  $\alpha$  and  $G$  that would be required for decreasing the wave amplitude by a factor of a fourth was then computed approximately using the amplification rates previously computed by the authors (Polymeropoulos & Gebhart 1966). A decrease in amplitude by a factor of a fourth was chosen because the resulting wave amplitude, two waves downstream from the ribbon, would be 0.00075 in., which, experience showed, could not be visually detected. Appendix C contains the expressions used in these computations.

The results are shown on figure 10. The short lines originating from the circles and half circles correspond to the paths of oscillations with initial  $\alpha$  and  $G$  conditions denoted by the circles and half circles. The ends of these lines indicate the computed  $\alpha$  and  $G$  values at the condition where the amplitudes have decreased by a factor of four. For all cases the length of these paths was less than one wavelength. The uncertainty thus computed indicates that there is probably better

agreement between the data from the approximate methods and the experimentally determined neutral stability curve than the agreement suggested by comparing the position of the data points (circles and half circles with the squares). It can therefore be argued that the data from the approximate method give a realistic approximation for the position of the neutral curve. It suggests an unstable region at low values of  $\alpha$  and  $G$  whose existence was predicted by Nachtshheim (1963) by taking into account the buoyancy coupling in his computations (curve  $b$  on figure 10).

#### *Discussion and conclusions*

An important result of this work is the effect on stability of the ribbon distance from the foil. This effect is illustrated on figure 4. The maximum frequency for amplification occurred for ribbon positions within 10% of  $\eta = 1.65$ , which is the location of the inflexion point of the base flow velocity profile. This point was therefore used as the ribbon distance from the foil for the neutral stability measurements.

Oscillations showing transition from damping to amplification, or vice versa, such as those shown on figures 6*c* and 6*d*, plate 1, respectively, establish beyond doubt the existence of a neutral stability curve for the free convection flow that was employed. Using such oscillations the experimental neutral curve in the range of  $182 < G < 515$  was located and is shown on figures 8 and 10. It is in good agreement with the previously computed neutral stability curves, even though it is located in the region predicted to be unstable by the theory. One possible reason for this discrepancy is the two-dimensional nature of the base flow which is evident by such effects as the change in oscillation wavelength with downstream position (figure 5). The stability computations were performed by assuming a one-dimensional base flow.

It was not possible to observe damping and subsequent amplification in the range of  $G < 182$  because of the necessarily small values of  $\alpha$  and  $G$  at the ribbon and the resulting long wavelengths. For example, assuming the neutral curve includes the point  $\alpha = 0.5$  and  $G = 150$  (figure 10), the ribbon would have to be at approximately  $\alpha = 0.7$  and  $G = 50$ . The curvature of the isotherms and the relatively long wavelengths at this position did not permit accurate measurements of wavelength and amplitude change.

The approximate methods did not require measurements of wave amplitude change. They could therefore be used to furnish stability information at low  $\alpha$  and  $G$  values, in the region where, for the reasons previously described, direct observation of transition from damping to amplification was not possible. For  $\alpha < 0.5$  and  $G < 125$  the results suggest the existence of an unstable region which is predicted unstable from computations with buoyancy coupling (curve  $b$  on figure 10), but is predicted stable from computations without buoyancy coupling (curves  $a$ ,  $c$  and  $d$  on figure 10). This shows that buoyancy coupling cannot be neglected for stability computations in the range of  $\alpha < 0.5$  and  $G < 125$ . However, the good agreement with experiment of the results of computations without buoyancy coupling for  $182 < G < 515$ , justify the use of uncoupled solutions at high values of  $G$ .

The authors wish to acknowledge the support of the National Science Foundation through grant GP 127 for this research.

### Appendix A

The base flow for free convection over a uniform flux plate is given by the following equations (Sparrow & Gregg 1956):

$$f''' - 3f'^2 + 4ff'' - H = 0, \quad (\text{A } 1)$$

$$H'' + Pr(4H'f - Hf') = 0, \quad (\text{A } 2)$$

where 
$$f' = \frac{5ux}{\nu G^2}, \quad H = \frac{(\Delta T)kG}{5q''x},$$

$$Pr = \frac{\mu c_p}{k}, \quad G = 5 \left[ \frac{Gr'_x}{5} \right]^{\frac{1}{2}}. \quad (\text{A } 3)$$

$\Delta T$  is the local plate temperature difference, and  $\mu$  is the dynamic viscosity. The derivatives are with respect to the similarity variable  $\eta = yG/5x$ .  $Gr'_x = g\beta q''x^3/k\gamma^2$  is the modified Grashof number for a uniform flux plate. The boundary conditions are:

$$\begin{aligned} \eta = 0, \quad f = f' = 0, \quad H' = 1; \\ \eta \rightarrow \infty, \quad f', H \rightarrow 0. \end{aligned}$$

### Appendix B

The conversion from the parameters  $\alpha$  and  $G$  to the corresponding parameters  $\alpha^+$  and  $G^+$  which are based on the average temperature difference ( $\Delta T$ ) for comparison with the results for the uniform temperature condition can be accomplished as follows:

$$\alpha^+ = \left[ \frac{2.5}{2.4}(-H_0) \right]^{-\frac{1}{4}} \alpha, \quad (\text{B } 1)$$

$$G^+ = \left[ \frac{3.2}{7.5}(-H_0) \right]^{\frac{1}{2}} G, \quad (\text{B } 2)$$

where  $(-H_0)$  is the non-dimensional temperature difference of the base flow at the plate surface,  $G^+ = 4[g\beta(\Delta T)x^3/4\nu^2]^{\frac{1}{2}}$  and  $\alpha^+ = 8\pi x/\lambda G^+$ .

### Appendix C

For a wave travelling along the foil the ratio of the amplitude between two positions  $x_1$  and  $x_2$  is given by

$$a_{12} = \exp \left\{ \int_{x_1}^{x_2} \alpha m dx \right\}, \quad (\text{C } 1)$$

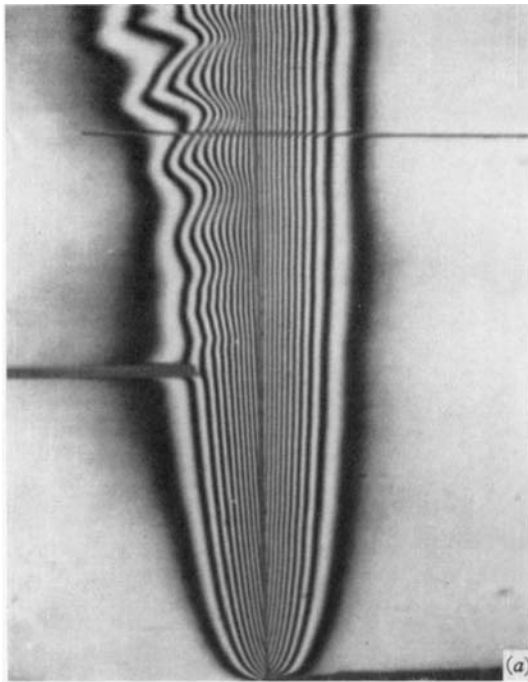
where  $a_{12}$  is the amplitude ratio and  $m$  is the ratio of the imaginary to the real parts of the phase velocity. Using (1), equation (B 1) can be integrated for constant  $m$  to give:

$$x_2^{\frac{2}{3}} - x_1^{\frac{2}{3}} = \frac{(\ln a_{12}) \nu f'(g\beta q''/5k\nu^2)^{\frac{2}{3}}}{\pi c m}. \quad (\text{C } 2)$$

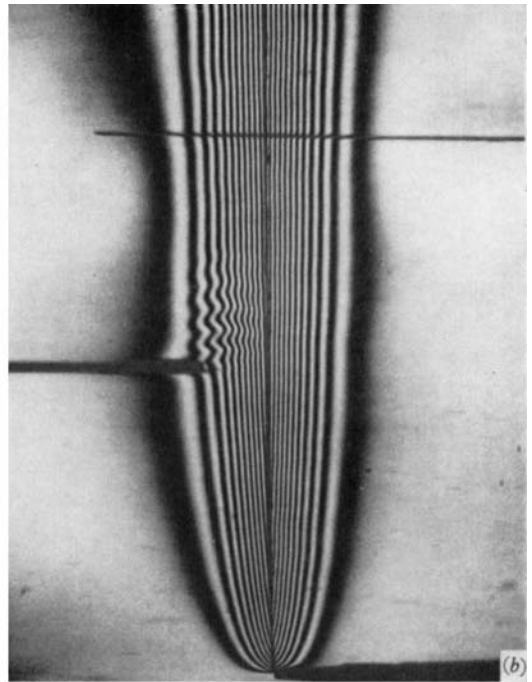
For a measured set of initial conditions (B 2), in combination with the definitions of  $\alpha$  and  $G$ , was used to compute the changes in  $\alpha$  and  $G$  along the lines on figure 10. For these cases  $a_{12}$  was taken to be 0.75 and  $m$  was given an average value of 0.0665.

## REFERENCES

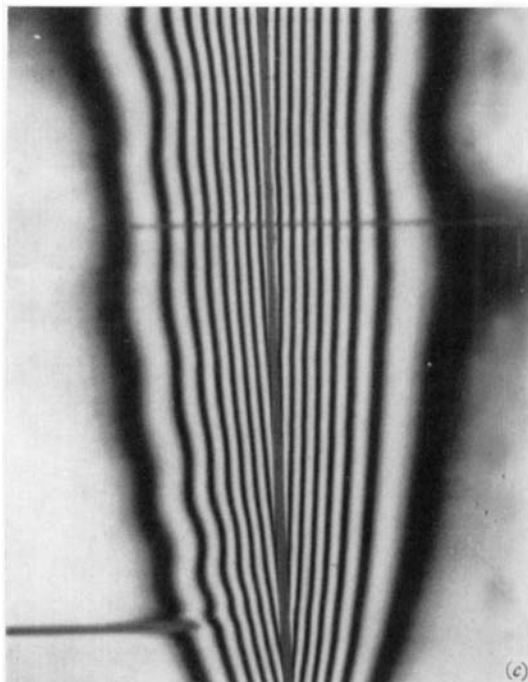
- BIRCH, W. D. 1957 M.S. Thesis, Air University.
- BUCHELE, D. R. & GOOSENS, H. R. 1954 *Rev. Sci. Instr.* **37**, 12.
- COLAK-ANTIC, P. 1964 *Jahrbuch der WGLR*, p. 171.
- ECKERT, E. R. G. & SOEHNGEN, E. E. 1951 *Proc. Gen. Disc. Ht. Tr. Lond.* p. 321.
- ECKERT, E. R. G., HARTNETT, J. P. & IRVINE, T. F. 1960 *ASME*, 60-WA-250.
- GARTRELL, H. E. 1959 M.S. Thesis, Air University.
- GEBHART, B. & KNOWLES, C. P. 1966 *Rev. Sci. Instr.* **37**, 12.
- HERMAN, R. 1936 *NACA TM*, 1366.
- HOLLMAN, J. P., GARTRELL, H. E. & SOEHNGEN, E. E. 1959 *WADD Tech. Rept.* **59**, 3.
- HOLLMAN, J. P., STOUT, K. E. & SOEHNGEN, E. E. 1960 *WADD Tech. Rept.* **60**, 24.
- KURTZ, E. F. & CRANDALL, S. H. 1961 *J. Math. Phys.* **41**, 1017.
- MORDCHELLES-REGNIER, G. & KAPLAN, C. 1963 *Proc. Ht. Tr. Fl. Mech. Inst.* **94**.
- NACHTSHEIM, P. R. 1963 *NASA TN D-2089*.
- POLYMEROPOULOS, C. E. 1966 Ph.D. Thesis, Cornell University.
- POLYMEROPOULOS, C. E. & GEBHART, B. 1966 *AIAA J.* **4**, 2066.
- SAUNDERS, O. A. 1939 *Proc. Roy. Soc. A* **172**, 55.
- SCHUBAUER, G. B. & SKRAMSTAD, H. K. 1948 *NACA Rept.* no. 909.
- SPARROW, E. M. & GREGG, J. L. 1956 *ASME Trans.* **78**, 435.
- SZEWCZYK, A. A. 1962 *Int. J. Ht. Mass Tr.* **5**, 903.



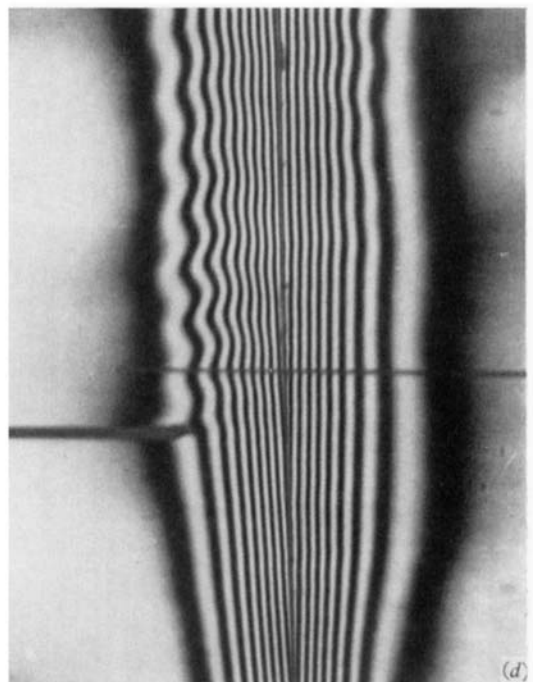
(a) Amplified,  $\alpha = 0.35$ ,  $G = 306$ .



(b) Damped,  $\alpha = 1.56$ ,  $G = 306$ .



(c) Damped-amplified,  $\alpha = 0.89$ ,  $G = 117$ .

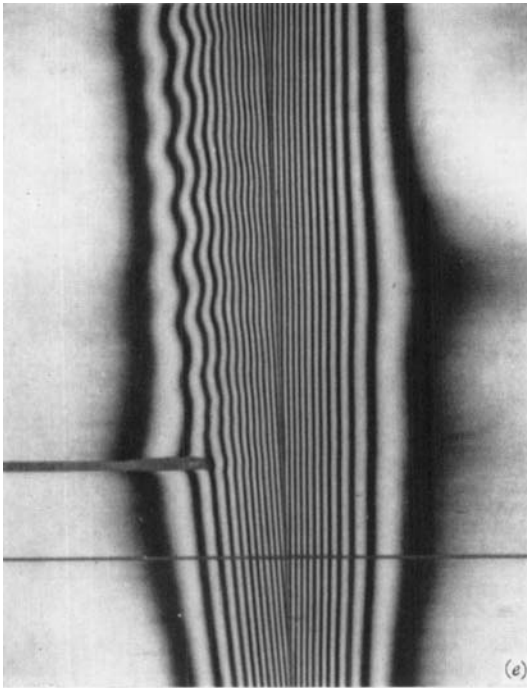


(d) Amplified-damped,  $\alpha = 0.92$ ,  $G = 378$ .

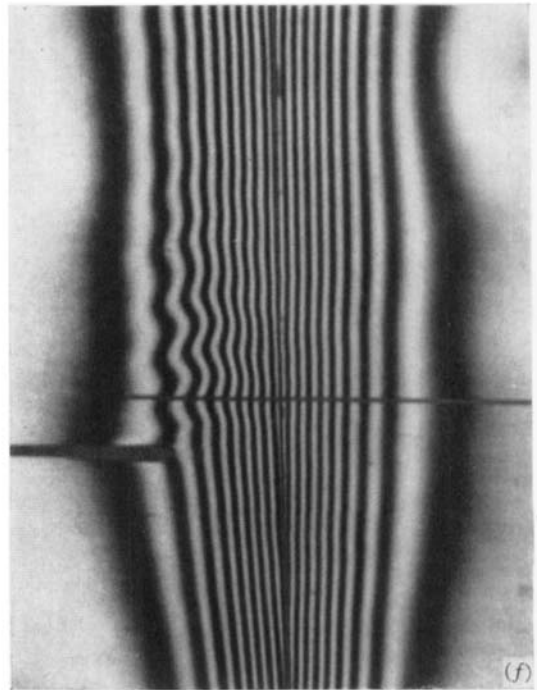
FIGURE 6. Interferograms of oscillations. Given values of  $\alpha$  and  $G$  are at the ribbon. The field is approximately 8 in. high and 1 in. wide.

POLYMEROPOULOS & GEBHART

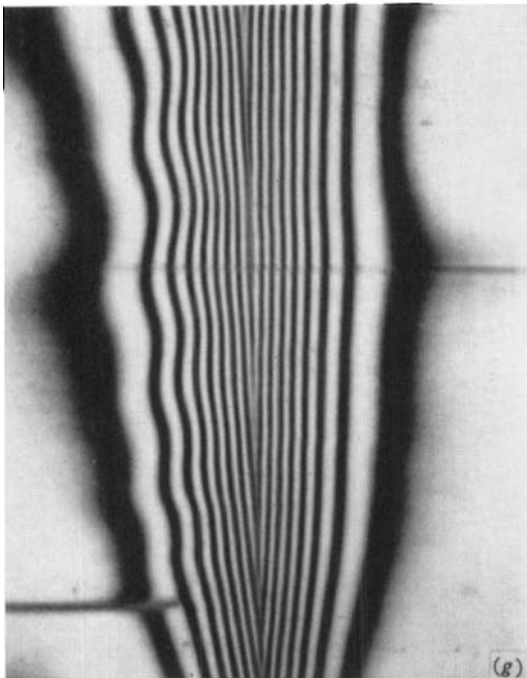
(Facing p. 340)



(e) Amplified,  $\alpha = 0.76$ ,  $G = 460$ .



(f) Damped,  $\alpha = 1.10$ ,  $G = 342$ .



(g) Amplified, originating near the neutral curve,  $\alpha = 0.64$ ,  $G = 342$ .